A Link-Layer Synchronization and Medium Access Control Protocol for Terahertz-Band Communication Networks

Qing Xia, *Student Member, IEEE*, Zahed Hossain, *Student Member, IEEE*, Michael Medley, *Senior Member, IEEE*, and Josep Miquel Jornet, *Member, IEEE*

Abstract—In this paper, a link-layer synchronization and medium access control (MAC) protocol for very-high-speed wireless communication networks in the Terahertz (THz) band is presented. The protocol relies on a receiver-initiated handshake to guarantee synchronization between transmitter and receiver. Two scenarios are considered, namely, a macroscale scenario, where nodes utilize rotating directional antennas to periodically sweep the space while overcoming the distance problem at THz frequencies, and a nanoscale scenario, where nano-devices require energy harvesting systems to operate. Both scenarios are implemented on a centralized and an ad-hoc network architecture. A carrier-based physical layer is considered for the macro-scenario, whereas the physical layer for the nano-scenario is based on a femtosecond-long pulse-based modulation scheme with packet interleaving. The performance of the proposed MAC protocol is analytically investigated in terms of delay, throughput and probability of successful packet delivery, and compared to that of an adapted Carrier Sense Multiple Access with Collision Avoidance (CSMA/CA) with and without handshake. The results are validated by means of extensive simulations with *ns*-3, in which all the necessary THz elements have been implemented. The results show that the proposed protocol can maximize the successful packet delivery probability without compromising the achievable throughput in THz-band communication networks.

Index Terms—Terahertz communications, MAC protocols, link-layer synchronization, ultra-broadband networking, 6G

1 Introduction

Over the last decade, wireless data traffic has drastically increased due to a change in the way today's society creates, shares and consumes information. More specifically, the global wireless mobile data traffic has grown 18-fold over the past 5 years [1]. This fast growth has been mainly caused by the booming usage of wireless devices, especially smart devices. It is estimated that wireless mobile data traffic will be seven times greater by 2021 than today. This change has been accompanied by an increasing demand for higher speed wireless communication *anywhere, anytime*. Following this trend, wireless multi-Gigabit-per-second (Gbps) and Terabit-per-second (Tbps) links are expected to become a reality within the next five years.

In this context, *Terahertz-band* (0.1 THz to 10 THz)[1] *communication* is envisioned as a potential wireless technology to satisfy the need for much higher wireless data rates [2], [3], [4], [5]. This frequency band, which lies in between millimeter wave (mmWave) and the far infrared, is still one of the least explored regions in the electromagnetic (EM) spectrum.

For many decades, the lack of compact high-power signal sources and high-sensitivity detectors able to work at room temperature has hampered the use of the THz band for any application beyond sensing. However, many recent advancements with several device technologies [6] are finally closing the so-called THz gap. In an *electronic approach*, the limits of standard silicon CMOS technology [7], silicon-germanium BiCMOS technology [8], III-V semiconductor HEMT [9], mHEMT [10], HBT [11], and Schottky diode [12] technologies are being pushed to reach the 1THz mark. In a *photonics approach*, uni-traveling carrier photodiodes [13], photoconductive antennas [14], optical downconversion systems [15] and quantum cascade lasers [16] are being investigated for high-power THz systems. More recently, the use of nanomaterials such as graphene is enabling the development of novel plasmonic devices for THz communications [17], [18]. These devices are intrinsically small, efficiently operate

- *Q. Xia is with the Sony Corporation of America, New York, NY 10022 USA. E-mail: qingxia@buffalo.edu.*
- *Z. Hossain is with the Intel Corporation, Santa Clara, CA 95052 USA. E-mail: zahedhos@buffalo.edu.*
- *J. M. Jornet is with Northeastern University, Boston, MA 02115 USA. E-mail: jmjornet@northeastern.edu.*
- *M. Medley is with the Air Force Research Laboratory/RITE, Rome, NY 13441 USA. E-mail: michael.medley@us.af.mil.*

Manuscript received 30 Dec. 2018; revised 24 July 2019; accepted 26 Aug. 2019. Date of publication 10 Sept. 2019; date of current version 3 Dec. 2020. (Corresponding author: Qing Xia.)
Digital Object Identifier no. 10.1109/TMC.2019.2940441

1. There are multiple terms to refer to the THz band, including *Tremendously High Frequencies*, *sub-millimeter waves*, and *Extreme Far Infrared*, with start frequencies as low as 100 GHz and as high as 10 THz. We adopt this broader definition.

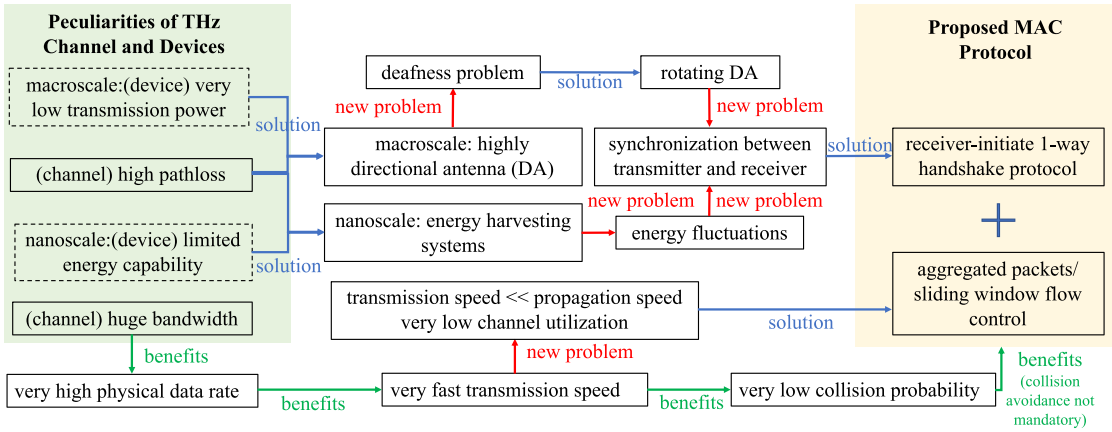

Fig. 1. Peculiarities of THz communication networks and the design logic.

at THz frequencies, and can support very large modulation bandwidths. Ultimately, whether in an electronic, photonic, plasmonic or even hybrid approach, THz communications are becoming a reality.

The THz band provides wireless communication devices with an unprecedentedly large bandwidth, ranging from several tens of GHz up to a few THz [19], [20]. The main phenomenon affecting the propagation of THz-band signals is the absorption by water vapor molecules. For communication distances below one meter (i.e., nanoscale scenarios), the THz band behaves as a single transmission window several THz wide. In contrast, for longer distances (i.e., macroscale scenarios), molecular absorption defines multiple transmission windows, each of them tens to hundreds of GHz wide. In both cases, physical-layer data-rates in the order of hundreds of Gbps and few Tbps have already been demonstrated, even with low-complexity modulations [21]. Thanks to the very large bandwidth at THz frequencies, THz devices do not need to aggressively contend for the channel. For instance, compared to both sub-6 GHz systems with up to 160 MHz bandwidth [22] as well as mmWave communication systems with up to 2.16 GHz bandwidth [23], the THz-band provides above hundred GHz of bandwidth in a single transmission window. In addition, the very high bit-rates enabled by such bandwidths lead to very short packet transmission times, which further minimizes the collision probability. For instance, with 100 GHz bandwidth, the time needed to transmit a packet of size 2000 bytes is only 160 ns, comparable to the propagation time.

In light of these results, a plethora of novel applications are enabled by THz-band communication [4], [24]. For macroscale scenarios, the advantage of the THz band comes mainly from the much larger available bandwidth. The corresponding applications include terabit wireless personal area networks, terabit small cells/wifi, secure ultra-broadband ultra narrow-beam communication links in the military and defense fields. For nanoscale scenarios, the advantage of the THz band comes mainly from the much smaller size of transceivers and antennas (enabled by the much shorter wavelength) in addition to the data-rates when needed. Thus, the application scenarios include intercore communication in wireless on-chip networks, wireless nanosensor networks for nuclear, biological and chemical defenses, and the Internet of Nano-Things.

However, the high path-loss at THz-band frequencies and the low transmission power of THz transceivers (from tens of microWatts [25] to tens of milliWatts [26]) introduce several challenges in terms of link-layer synchronization, which directly impact the achievable throughput of THz networks. On the one hand, in macroscale scenarios, highly directional antennas (DAs) are needed simultaneously in both transmission and reception all the time to establish wireless links beyond one meter. This is quite different with conventional communications, where omni-directional antennas are applied in at least one side of the communication links to achieve synchronization and beamforming. While directional communication can help to mitigate multi-user interference, it introduces the deafness problem [27], [28], [29]. This problem is the result of directional transmitting and receiving, leading to the signal strength at third party devices being too low to perform carrier sense. Moreover, the relatively long propagation delay when transmitting at Tbps over multi-meter-long links results in low channel utilization. On the other hand, while the issues caused by directional communication vanish in nanoscale applications, the limited energy capabilities of nano-devices requires them to use energy harvesting systems [30], which lead to severe energy fluctuations and, once again, impact the synchronization between the transmitter and the receiver.

To overcome these limitations, in this paper, we develop a link-layer synchronization and medium access control (MAC) protocol for very-high-speed wireless communication networks in the THz band. The protocol relies on a receiver-initiated handshake as a way to guarantee synchronization between the transmitter and the receiver. In addition, it incorporates an aggregated packet or a sliding window flow control mechanism, which combined with the 1-way handshake, maximizes the channel utilization. We summarize the peculiarities of THz-band communication and illustrate our design logic with a flowchart in Fig. 1.

We consider two different application scenarios: a macroscale scenario, in which nodes utilize high-speed rotating DAs to periodically sweep the space, and a nanoscale scenario, in which nodes use an energy harvesting nanosystem or power nano-generator. For each scenario, we consider different physical layers, namely, a traditional carrier-based modulation for the macroscale scenario and a femtosecond-long pulse-based modulation with user interleaving

for the nanoscale scenario. The waveform synchronization and symbol detection design for pulse-based communication has been demonstrated in [31]. Besides, for each scenario, we consider two different network architectures, namely, a centralized network architecture with one access point that always perform as a receiver while all other nodes perform as transmitters, and an ad-hoc network architecture, where all nodes are identical and periodically switch between receiver mode and transmitter mode.

We analytically investigate the performance of the proposed MAC protocol in terms of delay, throughput and successful packet delivery probability, and compare it to that of an adapted Carrier Sense Multiple Access with Collision Avoidance (CSMA/CA) protocol with and without handshake. The adapted CSMA/CA protocol takes into account the capabilities of the THz devices, i.e., the antenna's orientation in the macroscale scenario or the energy status in the nanoscale scenario. Finally, we implement in *ns*-3 [32] the proposed protocol and the necessary THz models (channel, carrier-based and pulse-based physical layers, rotating antenna and energy harvesting system), and provide extensive simulation results to validate our solution.

The remainder of this paper is organized as follows. We summarize the related work in Section 2. In Section 3, we describe the system model considered throughout the paper and derive formulations for the bit and packet error rates, the probability of collision in the macroscale and the nanoscale scenarios, the highly directional antenna in the macroscale scenario and the energy harvesting system for nano-devices. In Section 4, we describe the proposed protocol and, in Section 5, we analytically investigate its performance for the two scenarios. We provide simulation and numerical results in Section 6 and conclude the paper in Section 7.

2 Related Work

To the best of our knowledge, there are very few MAC protocols for THz-band communication. mmWave communications, which range from 30 to 300 GHz and provide multi-Gbps communication services, are considered as the closest existing technologies to THz-band communication in terms of frequency. Three major types of MAC protocols have been widely applied in mm-wave communication networks, which include CSMA/CA-based protocols, Time Division Multiple Access (TDMA)-based protocols and hybrid protocols. In this section, we summarize the advantages and drawbacks of these protocols and discuss the feasibilities of implementing these protocols in THz-band networks.

The drawbacks of TDMA-based protocols come from several aspects. First of all, for the centralized network architecture, the medium time for the bursty data traffic is often highly unpredictable. Thus, it is easy to under-flow allocate or over-flow allocate the medium time for each individual user. Besides, a huge number of control overheads are generated for the on-the-fly medium reservation, which, to some extent, defeat the original purpose of fast communication. Furthermore, it is challenging to implement a high-level computationally intensive and real-time executable access point (AP) or piconet coordinator (PNC) to schedule the burst traffic on a mobile device. Lastly, when it comes to the ad-hoc network architecture, it is even harder to achieve transmitter-receiver synchronization.

Comparing with TDMA-based protocols, CSMA/CA-based protocols work well with bursty traffic for both centralized and ad-hoc network architectures. However, conventional CSMA/CA-based protocols cannot adapt to the directional communication networks due to the challenging monitoring caused by the deafness problem. To overcome this issue, existing CSMA/CA-based protocols either utilize an omni-/quasi-omnidirectional to directional (O-to-D) antenna pairs to achieve beamforming and synchronization [28], [33], [34], [35], or utilize directional to directional (D-to-D) antenna pairs with caching the location information of all neighbor nodes on each sending device [36], the synchronization is established after sending multiple Directional Request-To-Send (DRTS) packets.

In addition to the deafness problem, the spatial interference is significantly reduced in the directional communication networks, thus, interference management or avoidance becomes a secondary consideration in MAC protocol design. For these reasons, the TDMA-based protocols, even suffering from the aforementioned drawbacks, are still widely used in the mmWave communication networks. However, the conventional TDMA protocol is very inefficient from the resource utilization point of view. Owing to the high degree of spatial diversity in mmWave communication networks, the time slots, which are used for data streaming in conventional TDMA protocol, can be further reused, i.e., one TDMA time slot can be occupied by several links which are determined to be not interfering each other. Thus, the spacial TDMA (STDMA)-based protocols [37] are proposed to improve the network efficiency.

In order to optimize the scheduling scheme for the STDMA-based protocol, works have been done in two aspects, which include heuristics solutions [38], in which O-to-D antenna pairs are utilized in the scheduling period; and analytical optimization solutions, within which the scheduling is achieved either by applying O-to-D antenna pairs [39] or by implementing the bootstrapping program [40], [41], such that the AP knows the up-to-date network topology and the location information of other nodes. Based on the extensive literature review, all the STDMA-based protocols, except for the protocols with bootstrapping program, need to implement the CSMA/CA protocols in the starting stage to achieve the synchronization, beamforming and scheduling, these implementations have also been presented in the corresponding IEEE standards.

There are mainly two existing IEEE standards for mmWave communication on 60 GHz band, which include the IEEE802.15.3c WPAN [42], [43], [44], [45] and the IEEE802.11.ad WLAN [46], [47]. IEEE802.11.ay [48], [49], an evolution of IEEE802.11.ad, is still under development. In all these standards, O-to-D antenna pairs are utilized in the scheduling period. In addition, hybrid MAC protocols are indicated in these standards. More specifically, in both IEEE802.15.3c and IEEE802.11.ad, the CSMA/CA protocol is mainly applied in the scheduling period, which is a contention-based access period. In contrast, the STDMA protocol is mainly utilized in the data exchanging period. Besides, polling is enabled for dynamic channel time allocation in IEEE802.11.ad.

However, the available solutions for lower-frequency systems cannot directly be utilized in a THz paradigm, mainly because they do not capture the peculiarities of the THz-band channel or the capabilities of THz devices. When it comes to the macroscale scenario, highly DAs are needed simultaneously in both transmission and reception sides all the time. Without implementation of O-to-D antenna pairs, the synchronization, scheduling and beamforming, again, become severe issues. Thus, the conventional CSMA/CA-based or TDMA-based protocols are not applicable for the macroscale scenario. Besides, due to the low transmission power of THz transmitters and the very high path-loss in the THz-band channel, it is infeasible to further divide the transmission power into different directions in one time slot. Thus, STDMA-based protocols are not feasible in the macroscale scenario as well. In [50], the authors proposed an assisted beamforming MAC protocol for THz communication networks, which exploits both 2.4 GHz and THz-band communication. In particular, the synchronization is achieved by using omnidirectional antennas that operate in 2.4 GHz channel, that support much slower transmission speeds than that in THz band. While functional, this system requires at least two radios.

When it comes to nanonetworks, THz devices utilize omni-directional antennas. The application of omni-directional antennas removes the deafness problem caused by directional communication. However, the devices lose the benefits of applying spatial reuse. Moreover, the THz devices suffer severe limitations in both memory and energy. Thus, the TDMA-based protocols, which either introduce a large number of control overheads or require a lot of memory to cache network information, are not feasible in THz-band nano-networks. In [51], the authors proposed the PHLAME, the first MAC protocol for ad-hoc nanonetworks. In this protocol, nano-devices such as nanosensors are able to dynamically choose different physical layer parameters based on the channel conditions and the energy of the nano-devices. Similarly, in [52], the authors proposed a centralized MAC protocol, in which a nano-controller would determine the best communication parameters for the nano-devices. In both cases, a transmitter-initiated hand-shake was required, which would eventually result in a low channel utilization. In [53], a receiver-initiated MAC protocol for nanosensor networks was proposed. The developed protocol is based on a distributed scheduling scheme, which requires the devices to perform a distributed edge coloring algorithm. However, due to the very limited computational resources of individual nano-devices, it seems more plausible to leverage the pulse-based physical layer to interleave users in time, rather than performing distributed scheduling algorithms [54].

This paper builds upon our preliminary work introduced in [55], where we proposed our receiver-initiated MAC protocol based on a infrastructure network architecture for two different application scenarios, namely, the macroscale scenario and the nanoscale scenario. In this paper, we have extended our work with our proposed MAC protocol to the ad-hoc network architecture, again for the two different application scenarios. Considering the complexity of the new scenario where each node can perform as both the transmitter and the receiver, allocating the resources efficiently in order to achieve the maximum throughput performance becomes a key problem.

3 THz-band Communication System Model

In this section, we summarize the main peculiarities of THz-band communication networks for both the macroscale scenario and the nanoscale scenario. Starting from an accurate THz-band channel model, we first formulate the Signal-to-Noise Ratio (SNR), which is needed for the computation of the Bit Error Rate (BER) and Packet Error Rate (PER) in both scenarios. Then, we formulate the collision probability in the macroscale scenario as well as in the nanoscale scenario, for which we review the concept of interleaved pulse-based transmissions. Next, we introduce the directional antenna model in the macroscale scenario and the energy model in the nanoscale scenario. Finally, we investigate both scenarios based on the *Centralized Network Architecture* and the *Ad-hoc Network Architecture*.

3.1 Signal-to-Noise Ratio

The propagation of electromagnetic waves at THz-band frequencies is mainly affected by molecular absorption, which results in both molecular absorption loss and molecular absorption noise. In particular, based on the THz-band channel model introduced in [19], the signal power at a distance d from the transmitter, P_r is given by:

$$P_r(d) = \int_B S_t(f)|H_c(f,d)|^2 G_t(f) G_r(f) df, \tag{1}$$

where S_t is the single-sided power spectral density (p.s.d) of the transmitted signal, B stands for its bandwidth and f refers to frequency. H_c represents the THz-band channel frequency response, which is given by:

$$H_c(f,d) = \left(\frac{c}{4\pi f d}\right) \exp\left(-\frac{k_{abs}(f) d}{2}\right), \tag{2}$$

where c refers to the speed of light and k_{abs} is the molecular absorption coefficient of the medium. k_{abs} depends on the molecular composition of the transmission medium, i.e., the type and concentration of molecules found in the channel and is computed as in [19]. G_t and G_r refer to the gain of transmitter antenna and receiver antenna, respectively.

Similarly, the molecular absorption noise power N_r at a distance d from the transmitter is modeled as additive, Gaussian, colored and correlated to the transmitted signal [56], which is given by:

$$\begin{aligned} N_r(d) &= \int_B S_{N_r}(f,d)|H_r(f)|^2 df \\ &= \int_B (S_{N^B}(f) + S_{N^I}(f,d))|H_r(f)|^2 df, \end{aligned} \tag{3}$$

where it is taken into account that the p.s.d. of the total molecular absorption noise N_r is contributed by the background atmospheric noise p.s.d., S_{N^B} and the self-induced noise p.s.d., S_{N^I}, which are computed as described in [56]. In addition, $H_r(f)$ refers to the receiver's impulse response.

The SNR at a distance d from the transmitter can be then obtained by dividing (1) by (3).

3.2 Bit Error Rate and Packet Error Rate

In this section, we derive the bit error rate (BER) and the packet error rate (PER) for the aforementioned two application scenarios according to their specific physical layers.

3.2.1 Macroscale Scenario

In the macroscale scenario, i.e., for distances above a few meters, we consider that nodes transmit a conventional QPSK modulated signal with the central frequency of 1.0345 THz (first absorption-defined window above 1 THz). This transmission window has a 3 dB bandwidth of 74 GHz at distance of 10 m.

For a given SNR, the BER, P_b, only depends on the modulation technique. Thus, the BER can be calculated as:

$$P_b = \frac{1}{2} erfc \sqrt{\frac{E_b}{S_{N_t}}}, \tag{4}$$

where E_b is the energy per bit and S_{N_t} is the total noise p.s.d, $erfc$ is the complementary error function. E_b/S_{N_t} represents a normalized SNR measure and is calculated as:

$$\frac{E_b}{S_{N_t}} = \frac{E_s}{2S_{N_t}} = \mathrm{SNR}\frac{B}{2R_s}, \tag{5}$$

where E_s stands for the energy per symbol in joules, R_s represents the symbol rate. Thus, the PER, P_p, can be expressed as:

$$P_p = 1 - (1 - P_b)^{L_p}, \tag{6}$$

where L_p refers to the packet length in bits.

3.2.2 Nanoscale Scenario

In the nanoscale scenario, i.e., for distances much below one meter, we consider that nodes transmit by using Time Spread On-Off Keying (TS-OOK), a modulation scheme based on the transmission of one-hundred-femtosecond-long pulses by following an on-off keying modulation spread in time [54]. The p.s.d. of such pulses is mainly contained between 0.9 and 4 THz.

To compute the BER and PER, we consider that a hybrid error control technique based on the combination of low-weight channel codes with ARQ is utilized, and we follow the same methodology as in [56]. As shown in the aforementioned work, the reduction of the coding weight (i.e., the number of "1"s in a codeword) can help to mitigate both the molecular absorption noise and the multi-user interference in nanonetworks and, thus, leads to a lower channel error probability. In this case, rather than retransmitting or trying to correct channel errors, the channel errors are prevented from happening in first instance.

3.3 Collision Probability

The collision probability in THz-band communication networks can be very low for the following two reasons. On the one hand, the spatial reuse in the macroscale scenario with highly DAs and the pulse-interleaving scheme in nanoscale scenarios reduce the probability of receiving two or more packets at the same time. On the other hand, the very fast transmission rate further decrease the transmission duration of packets and, thus, the collision vulnerable time. However, the collision probability is still one of the major reasons of transmission failure, especially for the long data (DATA) packets. In this section, we derive the collision probability for the two application scenarios.

3.3.1 Macroscale Scenario

In this case, nodes require high-gain DAs during both transmission and reception. To model the multi-user interference, we need to take into account both the spatial distribution of the nodes as well as their temporal activity. In our model, we consider that nodes are randomly distributed in space following a spatial Poisson process with rate λ_A. The area of influence of an individual node is given by $A(\Delta\theta) = \frac{\Delta\theta}{2\pi}\pi^2 = \frac{\Delta\theta^2}{2}$, where $\Delta\theta$ is the antenna beamwidth in radians which is derived in Section 3.4 and stands for the maximum transmission distance. Then, the probability of finding i nodes in A is given by:

$$P[i \in A(\Delta\theta)] = \frac{(\lambda_A A(\Delta\theta))^i}{i!} e^{-\lambda_A A(\Delta\theta)}. \tag{7}$$

If each node in A generates new packets at a rate given by $1/\alpha T_f$, where α is a constant and T_f stands for packet time, the aggregated traffic generated by i nodes is $\lambda_T = i/\alpha T_f$. Thus, the probability that j out of i nodes are active during a vulnerable time of $2T_f$ is given by:

$$P\big[j \in 2T_f\big] = \frac{\big(\lambda_T 2T_f\big)^j}{j!} e^{-\lambda_T 2T_f}. \tag{8}$$

Finally, the collision probability in the macroscale scenario is calculated as:

$$P_c = \sum_{i=1}^{\infty} P[i \in A(\Delta\theta l)]\big(1 - P\big[0 \in 2T_f\big]\big). \tag{9}$$

3.3.2 Nanoscale Scenario

In this case, miniature nodes do not require highly DAs, but transmit omnidirectionally. Therefore, the probability of finding i nodes in the area of influence of a node is given by (7) for $\Delta\theta = 2\pi$. This results in a much larger number of potentially interfering nodes. Interestingly, however, TS-OOK supports the simultaneous transmission and reception of time-interleaved packets. In this scheme, a logical "0" is transmitted as silence, whereas a logical "1" is transmitted with a pulse. The time between symbols, pulses and silences, T_s is much longer than the pulse duration T_p, $\beta = T_s/T_p \gg 1$.

By considering that each node i in A generates new packets at a rate $1/\alpha T_f$, the rate at which new pulses are generated is given by $\lambda_P = ip_1/\alpha T_s$, where p_1 refers to the probability of transmitting a pulse and is related to the coding weight [56]. Then, the probability of j out of i nodes generating pulses within the vulnerable time $2T_p$ is:

$$P\big[j \in 2T_p\big] = \frac{\big(\lambda_P 2T_p\big)^j}{j!} e^{-\lambda_P 2T_p}. \tag{10}$$

Finally, if there are n symbols in one packet, the collision probability of one packet in the nanoscale scenario is:

$$P_c = \sum_{i=1}^{\infty} P[i \in A(2\pi)]\left(1 - P\left[0 \in 2T_p\right]^n\right). \tag{11}$$

3.4 Macro Directional Antenna Model

In the macroscale scenario, highly DAs are applied to transmission and reception simultaneously to overcome high path loss. The antenna requirements are calculated by imposing the condition that the received signal strength should surpass the receiver sensitivity or minimum detectable signal strength at the receiver, i.e.,

$$\begin{aligned} &\int_B S_t(f)\frac{c^2}{(4\pi df)^2}e^{-k_{abs}(f)d}G_t(f)G_r(f)df \\ &\geq N_r(d)\mathrm{SNR}_{\min}, \end{aligned} \tag{12}$$

where $\mathrm{SNR}_{\min}$ stands for the minimum SNR threshold (10 dB in our analysis). From this, we derive the required antenna gain and resulting antenna beamwidth for the target transmission distance, transmitted signal power and the SNR threshold. Without loss of generality, in our analysis, we consider the antenna gains of the transmitter and the receiver to be identical and constant over the 3 dB frequency window, i.e., $G_t = G_r = G$. In this case, the desired antenna gain can be expressed as:

$$G \geq \sqrt{\frac{N_r(d)\mathrm{SNR}_{\min}}{\int_B S_t(f)\frac{c^2}{(4\pi df)^2}e^{-k_{abs}(f)d}df}}. \tag{13}$$

For highly DAs, the directivity gain can be approximated as [57]:

$$G \approx \frac{4\pi}{\Omega_A} = \frac{4\pi}{\theta_h \phi_h}, \tag{14}$$

where Ω_A refers to the array solid beam angle, and θ_h and ϕ_h are the Half Power Beam Width (HPBW) in the elevation plane and azimuthal plane, respectively. If we assume the HPBW in the elevation plane and azimuthal plane are identical, i.e., $\theta_h = \phi_h = \Delta\theta$, the beamwidth of the directive antenna can be calculated as follows:

$$\Delta\theta \leq \sqrt{4\pi\sqrt{\frac{\int_B S_t(f)\frac{c^2}{(4\pi df)^2}e^{-k_{abs}(f)d}df}{N_r(d)\mathrm{SNR}_{\min}}}}. \tag{15}$$

As we explain in Sections 4 and 5, the beamwidth plays a key role in the proposed solution.

In addition, the rotating highly DAs are applied in this scenario to prevent the deafness problem. The rotation of highly DAs can be achieved by either mechanically rotating a fixed pencil beam around the azimuth and elevation axes or by electronic beam steering with antenna arrays [58], [59], [60], [61] or lens arrays [62], [63]

3.5 Nano Energy Model

One of the main challenges in nanonetworks is posed by the very limited energy of nano-devices and their need for energy harvesting systems. Simply stated, a packet can only be successfully delivered if both the transmitter and the receiver have enough energy to do so. Given the fluctuations in the energy (as opposed to the always-decaying energy in non-harvesting battery-powered devices), the available energy needs to be stochastically modeled. In [64], the authors stochastically modeled the available energy for a nano-device by jointly taking the energy harvesting process when utilizing a piezoelectric nano-generator and the energy consumption process due to communication with TS-OOK. For this, the authors utilized a continuous-time Markov process to model the evolution of the nano-battery energy level. In our analysis, we utilize the same methodology to compute the packet error probability caused by insufficient energy at the transmitter or at the receiver.

In particular, the probability mass function (p.m.f.) of the energy stored at the nano-device battery after reaching a steady state depends both on the rate at which energy is harvested and the rate at which energy is consumed. The latter depends on the the new packet generation rate as well as on the expected number of retransmissions. Ultimately, different MAC protocols lead to different number of transmissions and, thus, into different p.m.f. for the energy at the nano-battery. With the p.m.f. of the energy, we can calculate the probability of having enough energy at each node.

In our study, we implement the harvesting model in *ns*-3 and utilize the collected data to estimate the battery p.m.f. used in our numerical results analysis. For the energy harvesting model, we implement an energy harvesting system that collects energy at a constant rate and provides interfaces to consume energy according to the packet length. To quantify the energy consumed in transmission and reception of a packet, we use the analysis provided in [64]. If we denote the energy consumed in transmitting an L bits packet as E_L^{tx} and energy consumed in receiving the same packet as E_L^{rx} , we obtain the following expressions:

$$\begin{cases} E_L^{tx} = \mathrm{LW}E_{pulse}^{tx} \\ E_L^{rx} = \mathrm{L}E_{pulse}^{rx}, \end{cases} \tag{16}$$

where E_{pulse}^{tx} and E_{pulse}^{rx} are the energy consumed in transmission and reception of a pulse respectively and W refers to the coding weight, i.e., the probability of transmitting a pulse instead of being silent. The energy consumed in the reception of a pulse E_{pulse}^{rx} is approximately 10 times lower than E_{pulse}^{tx}, which is a valid assumption for ultralow power transceivers [65].

3.6 Network Architecture

In our analysis, we are interested in the performance of the proposed protocol working on different network architectures for both the macroscale scenarios and the nanoscale scenarios.

3.6.1 Centralized Network Architecture

In this case, we assume that there is one access point (AP) performing as the receiver, and located at the center of the network. All other nodes are performing as transmitters and randomly distributed around the AP. This type of network architecture is relevant in small cell communications in 5G/6G cellular networks for macroscale scenarios. Also, it is consistent with the internet of Nano-Things envisioned architectures for nanoscale scenarios.

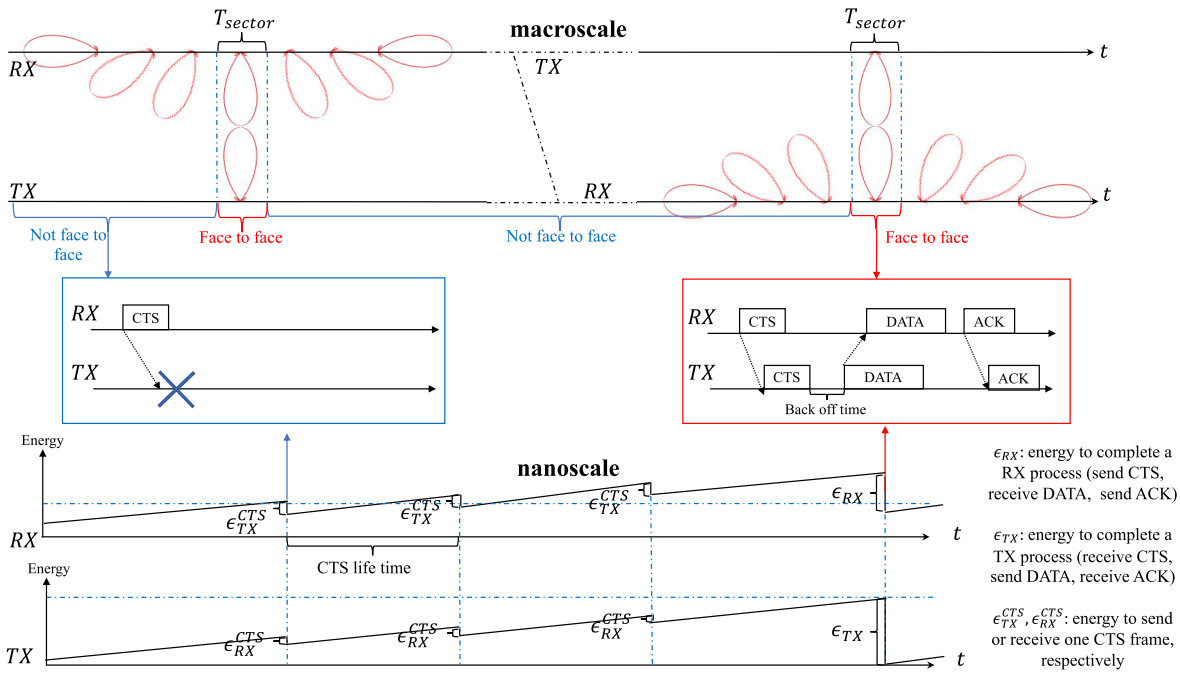

Fig. 2. Receiver-initiated 1-way handshake protocol.

3.6.2 Ad-hoc Network Architecture

In this case, we assume that all the nodes are equal and each node periodically switches between acting as a receiver or a transmitter. Since there is no AP, all nodes are randomly located within the maximum communication range. The corresponding application scenarios include the device to device communications in Terabit wireless personal area networks for macroscale scenarios, and the wireless on-chip communications for nanoscale scenario.

4 Receiver-Initiated Synchronization and Medium Access Control Protocol

In light of the system model described in Section 3, it is clear that a receiver-initiated handshake is needed in THz-band communication networks to guarantee link-layer synchronization between the transmitter and the receiver. The objective of such handshake is to prevent unnecessary data transmissions when the receiver is not available, whether because it is not facing the transmitter (macroscale scenario) or because it does not have enough energy to handle a new transmission (nanoscale scenario). The fundamental idea behind the proposed protocol is to reduce the overhead introduced by such handshaking process by having nodes announce their availability to receive data. In other words, the traditional 2-way handshake is reduced to a 1-way handshake process. Receiver-initiated MAC protocols have been successfully utilized in other scenarios [29], [53], [66], but the existing solutions cannot directly be utilized in our scenario because of the aforementioned peculiarities of THz-band communication networks.

Besides the 1-way handshake, the proposed protocol also makes use of an aggregated packet or a sliding window flow control at the link layer to maximize the channel utilization. In particular, both the delay introduced while waiting for the receiver availability and the relatively long propagation delay when transmitting at multi-Gbps or Tbps over multi-meter distances (macroscale scenario) result in a relative low channel utilization. To overcome such problems, the receiver can specify the time that it will remain facing in the current direction (macroscale scenario) or the amount of data packets it is willing to accept with its currently available energy (nanoscale scenario).

The basics of the protocol are summarized next. As shown in Fig. 2, a node can be found in transmitting mode or in receiving mode:

- A node in *transmitting mode (TM)*, i.e., with data to transmit, checks whether a current Clear-To-Send (CTS) packet from the intended receiver has been recently received. We consider that a CTS is valid for duration of antenna facing time in the macroscale scenario, or until the receiver is out of energy in the nanoscale scenario. The validity period of a CTS packet is termed as CTS life. If not, the node listens to the channel until the reception of a new CTS packet. In the macroscale scenario, we consider that the node in *TM* points its DAs to the receiver. For this, we consider that, at the link layer, the node in *TM* knows the position of the receiver [46]. This information is obtained during the neighbor discovery process, which could rely on heuristic methods such as those in [67], [68], or following innovative approaches such as the solution in [69], where expedited neighbor discovery in directional THz communication networks is achieved by leveraging antenna side-lobe information. In the nanoscale scenario, we consider that nodes utilize omni-directional antennas.
- A node in *receiving mode (RM)*, i.e., with sufficient resources (e.g., energy or even memory) to handle a new incoming transmission and with previous CTS life expired, broadcasts its status by means of a CTS packet. In the macroscale scenario, the node in *RM* uses a dynamically rotating narrow-beam to

broadcast CTS packets while sweeping its entire surrounding space. Such electrically controlled high-speed rotating DAs can be implemented [70], [71]. The node in *RM* mode cannot know in advance who is willing to transmit, which is why it needs to sweep the entire space. The rotating speed of the beam is a parameter to be optimized in our analysis. In the nanoscale scenario, this information is omnidirectionally transmitted.

Upon the reception of a CTS packet, a node in *TM* checks whether it has data for that receiver and the necessary resources. If so, it proceeds with the DATA packet transmission after waiting for a random backoff time. The random waiting time helps in avoiding collisions in the macroscale scenario. In the nanoscale scenario, it ensures that the energy is not wasted in transmitting more packets than the receiver can handle because the number of senders with data and sufficient resources is not known beforehand. If the transmission is successful, the node in *RM* sends a positive acknowledgement (ACK) packet. In the ACK packet, the receiver sets the flag that indicates if the CTS is still valid or not. If it is valid, the next node goes on to transmit its packet after the waiting time is over. If an acknowledgement is not received before the time-out, the node in *TM* will set a random back-off time, which depends on the number of transmission attempts, and repeats the entire process when done. After successfully receiving a packet, i.e., successfully transmitting a CTS, a DATA and an ACK packets, the node in *RM* can decide to keep rotating, continue to collect more packets, or switch to *TM*.

A couple of comments regarding *fairness* need to be made. First, as in any triggered reaction protocol, nodes in *TM* wait a random time after receiving a CTS packet and before sending the DATA packet. In the macroscale scenario, carrier-sense is performed during that time. In the nanoscale scenario, in which a pulsed-based physical layer is used, there is no carrier to sense, but the chances of having a collision are very low (Section 3). Second, only for the macroscale scenario, since the receiver's DA keeps "rotating", we need to guarantee that the DATA packet can be successfully transmitted within the small span of the facing time of transmitter's DA and receiver's DA. This is possible because nodes are transmitting at multi-Gbps and even Tbps and, thus, only several nanoseconds are usually needed.

5 Performance Analysis

In this section, we analytically investigate the performance of the proposed protocol in terms of successful packet delivery probability, packet delay and throughput. The analysis is based on both network architectures (centralized, ad-hoc) and application scenarios (macro, nano). In the centralized network architecture, we analytically investigate the impact of the AP performance (e.g., antenna rotating speed, energy harvesting rate) on the system performance. In the ad-hoc network architecture, we study the resource allocation strategy, such as the *TM* duration and the *RM* duration allocation for the macroscale scenario and transmission energy and reception energy allocation for the nanoscale scenario. In both network architectures, we first focus on the macroscale scenario and develop a mathematical framework in detail. Then, we summarize the differences needed to capture the nanoscale scenario peculiarities.

5.1 Centralized Network Architecture

5.1.1 Macroscale Scenario

In this case, the AP in the *RM* keeps rotating the beam to sweep through the entire circle while the rest of nodes in the *TM* point their beams toward the AP. Thus, the number of sectors within one antenna rotating circle is:

$$N_{sector} = \frac{2\pi}{\Delta\theta}. \tag{17}$$

The main factor affecting the performance of the protocol is the antenna rotating speed ω, given in circles-per-second. In particular, we consider that the antenna shifts its direction in discrete steps and, thus, provides coverage to different sectors in different times. We define the sector time or time during which the antenna beam is pointing to a certain direction as $T_{sector} = \Delta\theta/(2\pi\omega)$. Simply posed, at least one DATA packet needs to be successfully transmitted from the transmitter within one sector time of the rotating antenna. T_{sector} needs to guarantee a complete transmission process starting with sending out the CTS for our designed protocol, thus we have:

$$T_{sector} = \frac{L_{\mathrm{CTS}}}{R} + T_{prop} + \frac{L_{\mathrm{DATA}}}{R} + T_{prop} + \frac{L_{\mathrm{ACK}}}{R} + T_{guard}, \tag{18}$$

where $L_{\mathrm{CTS}}, L_{\mathrm{DATA}}$ and L_{ACK} refer to the packet length (in bits) of CTS packet, DATA packet and ACK packet, respectively. T_{prop} stands for the propagation duration, and R is the data rate of the selected 3 dB frequency window. T_{guard} is the guard time.

The best case scenario is when a successful transmission is directly achieved without any retransmissions during the time the beams of the transmitter and the receiver face each other. By applying the shortest sector time T^{min}_{sector} from (18), the maximum throughput can be calculated as a function of the DATA packet length in bits L_{DATA}:

$$S_{max} = \frac{L_{\mathrm{DATA}}}{T^{min}_{sector} N_{sector}}. \tag{19}$$

We observe that the higher S_{max} will be achieved with a larger L_{DATA}.

In the general case, T_{sector} limits the maximum number of retransmissions that a node can complete in the current round, s. This affects the overall packet delay and throughput, as the node will have to wait for an entire cycle before being able to continue its ongoing transmission in round, $s+1$. More specifically, the maximum number of retransmission, η_{max}, that a node can complete in round, s, can be calculated as follows:

$$\eta_{max}[s] = \min\left\{ \left\lfloor \frac{T_{sector} - T_{\mathrm{CTS}} - T_{prop}}{T_{t/o} + T_{b/o}} \right\rfloor, k[s] \right\}, \tag{20}$$

where $T_{t/o} = 2T_{prop} + T_{proc} + T_{\mathrm{DATA}} + T_{\mathrm{ACK}}$ is the time-out duration, T_{CTS}, T_{DATA} and T_{ACK} refer to the CTS, DATA,

and ACK packets transmission time, respectively, and $T_{b/o}$ is a random exponential back-off time. In our analysis, we do not ignore the impact of the propagation delay, T_{prop}, as it is comparable or even larger than the packet transmission time in the macroscale scenario. k stands for the maximum number of retransmissions available in the current round. In particular, $k[1]$ is set to a default value k_0, which is the maximum number of retransmissions across rounds. For example, if $k_0 = 5$, the total amount of retransmissions for a specific packet is equal to 5. This can be "consumed" within one round if T_{sector} is very long, i.e., the antenna turns at a slow speed or might be spread across rounds, otherwise.

Then, the probability to succeed with exactly i retransmissions within the same round is given by:

$$P_{succ}^{i-rtx} = P_{\text{CTS}}(1 - P_{\text{DATA}}P_{\text{ACK}})^{i-1}P_{\text{DATA}}P_{\text{ACK}}, \tag{21}$$

where $P_{\text{CTS}} = \overline{P_p} = \big(1 - P_p\big)$, which is the probability of successfully receiving a CTS packet; If not specified, the function $\overline{P}$ is defined as $1 - P$ in the rest of our paper. $P_{\text{DATA}} = \overline{P_c}\ \overline{P_p}$ is the probability of successfully receiving a DATA packet; $P_{\text{ACK}} = \overline{P_p}$ is the probability of successfully receiving an ACK packet, where P_p and P_c refer to the PER and the collision probability, respectively, as we derived in Section 3. We consider that the main reason for not properly receiving the CTS is the presence of bit errors, rather than the collision with other CTS. In the macroscale scenario, this is generally true, as it is unlikely to have two or more receivers located inside the same sector area of a transmitter and pointing their directional beams toward the transmitter simultaneously. Similarly, in the nanoscale scenario, given the energy constraints of nano-devices, it is not likely to have many nearby receivers announcing their availability at the same time. When it comes to the DATA packet, failures might occur because of both bit errors as well as collisions. Even if we introduce a random initial delay between the CTS reception and the DATA transmission, collisions can occur. Finally, ACK packets might also suffer from bit errors.

From this, we can easily write the probability to successfully transmit the packet P_{succ}^{rnd} in round s as well as the expected number of retransmissions η in that round as:

$$P_{succ}^{rnd}[s] = \sum_{i=1}^{\eta_{max}[s]} P_{succ}^{i-rtx}; \quad \eta[s] = \sum_{i=1}^{\eta_{max}[s]} iP_{succ}^{i-rtx}. \tag{22}$$

If successful, the average successful packet delay introduced by the current round s can be calculated as:

$$T_{succ}[s] = (\eta[s] - 1)\big(T_{t/o} + T_{b/o}\big) + T_{succ}^{1}, \tag{23}$$

where $T_{succ}^{1} = 2T_{prop} + T_{proc} + T_{\text{DATA}} + T_{\text{ACK}}$ is the delay when successfully transmitting the packet in one attempt.

If the node is not successful in the current round, but k_0 has not been yet achieved, the node waits for a new CTS packet (after one antenna cycle). Now $k[s+1] = k[s] - \eta^{max}[s]$. The maximum number of rounds Γ_{max} is given by

$$\Gamma_{max} = \min_s\{k[s] = 0\}. \tag{24}$$

Then, the probability to successfully transmit a packet in the jth round is given by:

$$P_{succ}^{j-rnd} = \left(\prod_{u=1}^{j-1}\big(1 - P_{succ}^{rnd}[u]\big)\right)P_{succ}^{rnd}[j], \tag{25}$$

where P_{succ}^{rnd} is given in (22).

From this, the total packet successful delivery probability and the average number of rounds needed to do so are given by:

$$P_{succ} = \sum_{j=1}^{\Gamma_{max}} P_{succ}^{j-rnd}; \quad \Gamma = \sum_{j=1}^{\Gamma_{max}} jP_{succ}^{j-rnd}. \tag{26}$$

The discard probability immediately follows as $P_{dis} = \overline{P_{succ}}$. The average packet delay can similarly be obtained as:

$$T_{packet} = \sum_{j=1}^{\Gamma_{max}}\prod_{u=1}^{j-1}\big(1 - P_{succ}^{rnd}[u]\big)P_{succ}[j] \big((j-1)T_{cycle} + T_{succ}[j]\big) + T_{wait}, \tag{27}$$

where T_{cycle} is the time needed for the antenna to complete one entire circle. T_{wait} refers to the average time that the transmitter will have to wait for the receiver's CTS in the first round, and is computed as follows:

$$T_{wait} = \sum_{i=1}^{n_{sectors}} \overline{P_f}^{(i-1)}P_f(i-1)T_{sector}, \tag{28}$$

where $n_{sectors} = 2\pi/\Delta\theta$ is the number of sectors and $P_f = \Delta\theta/\pi$ is the transmitter and receiver facing probability. Finally, we can obtain the throughput as $S = n_{packet}/T_{packet}$, where n_{packet} is the number of bits per packet.

5.1.2 Nanoscale Scenario

In this case, the main problem affecting the performance of the protocol is posed by the fluctuations in the available energy in each nano-device, which were discussed in Section 3.5. In our analysis, we consider that the battery in each nano-device can hold up to ϵ_{max} energy packets, where ϵ_{max} is the maximum energy packet limitation for each nano-device. An energy packet is the energy in Joules consumed in the reception of a control packet (CTS or ACK), also denoted as $\epsilon_{control}^{rx}$. Similarly, $\epsilon_{control}^{tx}$ denotes the energy packets required to transmit a control packet, and $\epsilon_{\text{DATA}}^{tx}$ and $\epsilon_{\text{DATA}}^{rx}$ are the number of energy packets needed to transmit and receive a DATA packet, respectively. The rate at which energy packets are harvested is denoted by λ_{harv}. Based on the probability distribution of the battery energy status, as described in Section 3.5, we can calculate the insufficient energy probability and its impact on the system.

The model now is fundamentally the same, with only a few modifications. In this case, the reception of a CTS packet is not governed by the antenna rotating speed, ω, and the sector time, T_{sector}, but by the time needed by the receiver to harvest enough energy to operate and announce its availability by broadcasting a CTS. Upon the reception of a CTS packet, the node in *TM* checks whether it has enough energy to successfully transmit a packet. The new

maximum number of transmissions, η_{max}, in round, s, is given by:

$$\eta_{max}[s] = \min\Bigg\{\left\lfloor \frac{\mathrm{CTS}_{life}}{T_{t/o}+T_{b/o}}\right\rfloor, k[s], \left\lfloor \sum_{i=\epsilon^{tx}}^{\epsilon^{max}} P[level=i]\left\lfloor \frac{i-\epsilon^{tx}}{\epsilon_{retry}}\right\rfloor +1\right\rfloor\Bigg\}, \tag{29}$$

where CTS_{life} refers to the CTS packet lifetime, set by the receiver according to its energy; $T_{t/o}$ and $T_{b/o}$ are the time-out and back-off times, respectively, defined similarly as for the macroscale scenario; $\epsilon^{tx} = \epsilon^{rx}_{\mathrm{CTS}} + \epsilon^{tx}_{\mathrm{DATA}} + \epsilon^{rx}_{\mathrm{ACK}}$ is the energy required to complete a packet transmission on the transmitter side; *level* is the number of energy packet units contained in the battery; and ϵ_{retry} is the energy spent in a retransmission. As before, k is a parameter value that specifies the maximum number of transmissions still available.

In general, there is no guarantee that the transmitter and the receiver will have enough energy to successfully complete the packet transaction in one round, i.e., during the duration of the current CTS lifetime. As a result, both nodes might have to wait until they have harvested the required energy. The average waiting times for the transmitter and the receiver nodes are given by:

$$T^{tx/rx}_{wait} = \frac{1}{\lambda_{harv}} \sum_{i=0}^{\epsilon^{tx/rx}} P[level=i]\Big(\epsilon^{tx/rx} - i\Big), \tag{30}$$

where $\epsilon^{rx} = \epsilon^{tx}_{\mathrm{CTS}} + \epsilon^{rx}_{\mathrm{DATA}} + \epsilon^{tx}_{\mathrm{ACK}}$ is the required energy to start transmission from the receiver side. Thus, the average waiting time for the packet transmission can be calculated as:

$$\begin{aligned} T_{wait} = {} & P^{tx}_{wait}\overline{P^{rx}_{wait}}T^{tx}_{wait} + \overline{P^{tx}_{wait}}P^{rx}_{wait}T^{rx}_{wait} \\ & + P^{tx}_{wait}P^{rx}_{wait}\ \max\{T^{tx}_{wait}, T^{rx}_{wait}\}, \end{aligned} \tag{31}$$

where

$$P^{tx}_{wait} = \sum_{i=0}^{\epsilon^{tx}} P[level=i];\ P^{rx}_{wait} = \sum_{i=0}^{\epsilon^{rx}} P[level=i], \tag{32}$$

are the waiting probability for the transmitter and the receiver, respectively. The packet delay T_{packet} can be now obtained by utilizing (31) in (27) instead of (28). The rest of the analytical model remains the same.

5.2 Ad-hoc Network Architecture

5.2.1 Macroscale Scenario

In this case, each node switches between *TM* and *RM* periodically. The main problem is to reasonably allocate *TM* time and *RM* time of each node in order to guarantee the maximum network throughput. On the one hand, more *TM* time assigned to each node may lead to a selfish network, in which every node wants to contend for the channel without announcing its availability to receive DATA. As a result, there are a few nodes that can send out their own DATA packet. On the other hand, a very generous network will be created by allocating more *RM* time for each node. In this case, every node will patiently wait for others' DATA instead of sending out their own DATA. In both cases, an increasing amount of DATA packets will be stored in each node's buffer during the communication progress and, thus, lead to an increased average delay.

We first analyze the two-node case and then generalize it for the multiple-node case. In our analysis, the randomness in the scenario is introduced by the geographical distribution and the time resource allocation of each node. The generalization to the multi-node scenario is possible because, in terms of network topology, the transmitter and receiver always face each other once within one steering-cycle of a receiver's DA, and this is achievable irrespective of their locations. In terms of resource allocation, the generalization is also possible by randomly distributing the operation mode starting time of each nodes following a Poisson distribution in our analysis.

For the ad-hoc network architecture, other than the *directivity matching* factor we have seen in the centralized network architecture, *mode matching* is another factor that affects the network throughput. The maximum network throughput is achieved when the mode matching probability of all nodes is the highest.

In the two-node case, we denote the nodes as node i and node j. We define one mode cycle as the summation of a *TM* duration and a *RM* duration, i.e., $T_{cycle} = T_{TM} + T_{RM}$. In the best case, one DATA packet is successfully sent out within one packet generation interval, which is calculated as:

$$\lambda_Q \le \frac{1}{T_Q} = \frac{1}{T_{cycle}}, \tag{33}$$

where T_Q refers to the enqueue interval of the DATA packet and, thus, λ_Q is the enqueue rate of the DATA packet.

We assume that, for each node, *RM* occurs at least once during T_Q with an occurring rate λ_{RM}:

$$\lambda_{RM} = \lambda_Q \frac{T_{RM}}{T_Q} = \frac{1}{T_Q}\frac{T_{RM}}{T_Q} = \frac{T_{RM}}{T_Q^2} = \frac{T_{RM}}{(T_{TM}+T_{RM})^2}. \tag{34}$$

The probability that the mode of node i matches the mode of node j can be calculated as:

$$P^{i-j}_{match} = \frac{\lambda^i_{RM}T^j_{TM}}{1!}e^{-(\lambda^i_{RM}T^j_{TM})}, \tag{35}$$

where λ^i_{RM} refers to the occurring rate of RM of node i and T^j_{TM} refers to the duration of *TM* of node j. Since the allocation scheme of mode duration should be same for each node, we have $T^i_{TM} = T^j_{TM}$. The probability of mode matching function can be simplified by utilizing this statement and inserting (34) in (35), thus:

$$P^{i-j}_{match} = \frac{\eta}{(1+\eta)^2}e^{-\frac{\eta}{(1+\eta)^2}}, \tag{36}$$

where $\eta = \frac{T_{RM}}{T_{TM}}$ is the ratio of *RM* duration to *TM* duration. The maximum network throughput can be achieved when the mode matching probability P^{i-j}_{match} is maximum. By taking the derivative of P^{i-j}_{match} with respect to η and set it equal to zero, we find the solution $\eta = 1$, which means *TM* duration and *RM* duration should be equally allocated in a two nodes case to achieve the maximum throughput.

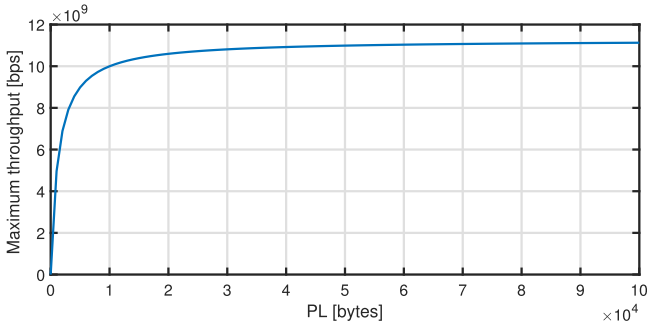

Fig. 3. Maximum throughput as a function of the DATA packet length.

The analysis of the three nodes case follows the same logic. We denote the nodes as m, n and j and the development of our analysis is based on node j. When node m and node n perform in the same mode, it will be very similar to the basic two nodes case. Hence we study the case while node m and node n always perform differently. So the mode matching probability corresponding to node j can be represented as:

$$P_{match}^{m,n-j} = P_{match}^{m-j} P_{match}^{n-j} = \lambda_{RM}^{m} T_{TM}^{j} e^{-\lambda_{RM}^{m} T_{TM}^{j}} \lambda_{TM}^{n} T_{RM}^{j} e^{-\lambda_{TM}^{n} T_{RM}^{j}}, \tag{37}$$

with the concept of λ_{RM} we defined in (34), we can easily calculate the occurring rate of *TM* as:

$$\lambda_{TM} = \frac{T_{TM}}{(T_{TM} + T_{RM})^2}. \tag{38}$$

We assume node m and node n have the same mode allocation ratio so that: $\lambda_{TM}^{m} = \lambda_{TM}^{n} = \lambda_{TM}$ and $\lambda_{RM}^{m} = \lambda_{RM}^{n} = \lambda_{RM}$. The mode matching probability can be simplified by applying this assumption and inserting (34) and (38) in (37), leading to

$$P_{match}^{m,n-j} = \frac{\eta^2 + \eta - \eta\eta'}{(\eta+1)^2} e^{-\frac{\eta^2+\eta-\eta\eta'}{(\eta+1)^2}} \frac{\eta'}{(\eta+1)^2} e^{-\frac{\eta'}{(\eta+1)^2}}, \tag{39}$$

where $\eta' = \frac{T_{RM}^{j}}{T_{TM}}$, which refers to the ratio of *RM* duration of node j to *TM* duration of node m or node n. $\eta = \frac{T_{RM}}{T_{TM}}$, which refers to the ratio of *RM* duration to *TM* duration of node m or node n. The maximum $P_{match}^{m,n-j}$ occurring at $\eta = 1$ and $\eta' = 1$, which means in order to guarantee the maximum network throughput in this case, we need to allocate equal *RM* duration and *TM* duration for each node.

When the scenario extends to the multiple nodes case, we consider it is consisted of different combinations of the two nodes case and the three nodes case. The mode probability can be calculated as:

$$P_{match}^{X,Y-j} = \sum_{x=1,y=k-x-1}^{x+y=k-1} \frac{\eta^{k-1}}{(1+\eta)^{2(k-1)}} e^{-\frac{(k-1)\eta}{(\eta+1)^2}}, k \geq 2, \tag{40}$$

where X and Y represent two groups of nodes performing different modes, x and y stand for the number of nodes in each group correspondingly, k is the total number of nodes including node j, and η refers to the ratio of *TM* duration to *RM* duration of each node. Based on numerical analysis, the highest mode matching probability always occurs at $\eta = 1$, which suggest to us to equally allocate time resource during one mode cycle.

5.2.2 Nanoscale Scenario

The main difference in the ad-hoc architecture from the centralized case is that each node can perform *TM* and *RM* simultaneously. That is, a node can transmit and receive at the same time with the help of pulse interleaving if it has sufficient energy. However, when there is not sufficient energy, the node needs to decide whether it should receive while waiting to harvest enough energy to transmit. Is it more efficient to send a CTS as soon as the node harvests ϵ^{rx} amount of energy or wait till $\epsilon^{rx} + \epsilon^{tx}$ energy is harvested? The node has the option of sending the CTS packet when its energy level is anywhere between ϵ^{rx} and $\epsilon^{rx} + \epsilon^{tx}$. The best decision can be derived by minimizing T_{wait} with respect to ϵ^{rx}. However, for this, we need to express the energy distribution in terms of ϵ^{rx} which is a complex process as developed in [64]. Hence, we derive the best decision numerically in this paper.

6 Simulation Results

In this section, we investigate the performance of the proposed protocol in both centralized and ad-hoc network architectures and compare it to that of adapted CSMA/CA with and without RTS/CTS (2-way and 0-way handshake). The numerical results obtained by solving the analytical models developed in Section 5 are validated by network simulations with *ns*-3. For this, we have implemented in *ns*-3 the frequency-selective THz-band channel, the two THz physical layers (carrier-based and pulse-based with interleaving), the high-speed turning antenna model, the energy harvesting unit and our proposed protocol, and we have also tailored CSMA/CA to work with the THz models. The resulting platform, which we refer to as TeraSim [72], is free to download and has been contributed to the *ns*-3 application store. For each point of our simulation results, we completed 50 simulations based on different seed numbers. For each simulation test, more than 200 DATA packets have been transmitted from each node.

6.1 Macroscale Scenario

In our analysis, nodes communicate at $f_c = 1.03$ THz over a 3 dB frequency window with $B = 74$ GHz at 10 m. The transmitted power P_t is set to -20 dBm, and the minimum Signal-to-Noise Ratio ($\mathrm{SNR_{min}}$) is 10 dB, while the background noise N_r equals -110 dBm. The received power strength threshold P_{RXmin} is set as -100 dBm. In this case, the required antenna gain is 17.3 dB, and the beam width is 27.7°. Nodes utilize QPSK modulation, for which the unique number of symbols is M=4 and, thus, the bit rate is $R = 148$ Gbps. To maximize the theoretical throughput, given by (19), we set the DATA packet length to $L_{\mathrm{DATA}} = 15,000$ bytes. As shown in Fig. 3, the achievable maximum throughput does not further increase for longer packets. The turning DA sweeps its entire surrounding space sector by sector, with $T_{sector}^{min} = 879.26$ ns for 1-way protocol, $T_{sector}^{min} = 913.5$ ns for 2-way and $T_{sector}^{min} = 845.0$ ns for 0-way, with N_{sector}=13. In this case, $T_{circle} = 11430.4$ ns for 1-way, and 11875.5 ns and 10985.1 ns

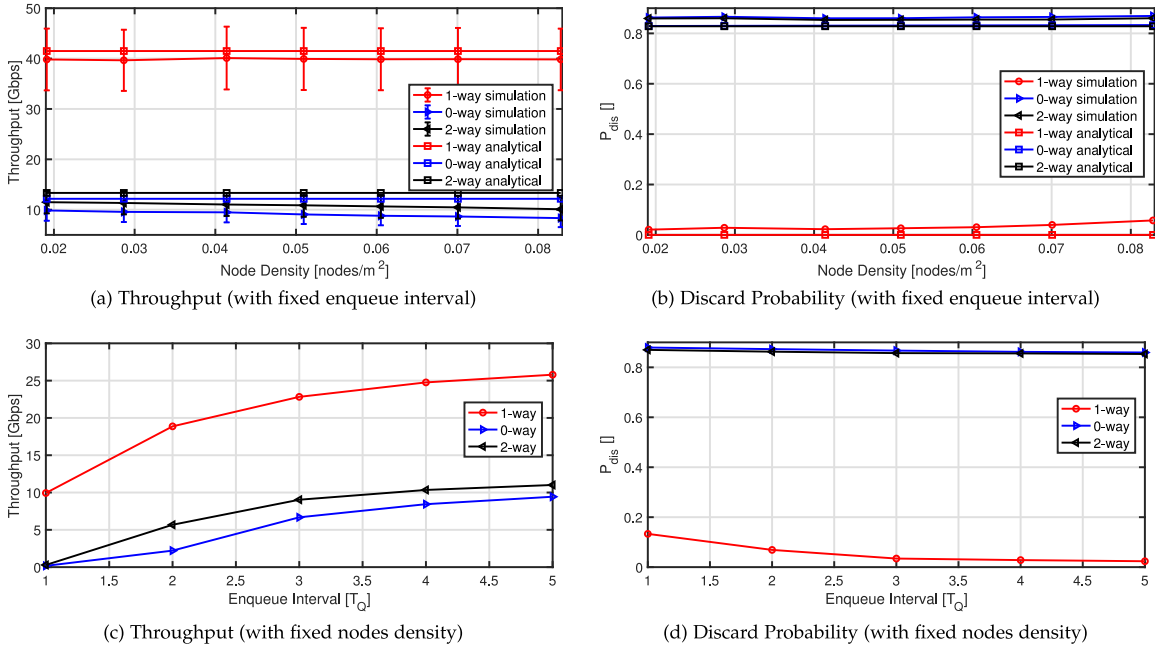

(a) Throughput (with fixed enqueue interval)

(b) Discard Probability (with fixed enqueue interval)

(c) Throughput (with fixed nodes density)

(d) Discard Probability (with fixed nodes density)

Fig. 4. Centralized network architecture: Throughput and discard probability.

for 2-way and 0-way, respectively. In order to guarantee the transceivers can meet each other, T_{RM} needs to be smaller than T_{circle}. Packet enqueue duration $T_Q \geq 2T_{circle} = 22.86\ \mu s$ for 1-way, $23.75\ \mu s$ for 2-way and $21.97\ \mu s$ for 0-way, and the antenna rotates at 87486.4 round/s, 842067.0 round/s and 91032.04 round/s respectively for the 1-way, 2-way and 0-way protocols.

6.1.1 Centralized Network Architecture

In Figs. 4b and 4d, the DATA packet discard probability of our proposed receiver-initiated or 1-way handshake protocol is shown as a function of node density and DATA packet enqueue interval. It is apparent that a denser network or a faster DATA packet enqueue rate could lead to more aggressive network contention and, thus, higher DATA packet discard probability. As expected, with the proposed 1-way handshake protocol, the probability of discarding a packet is much lower than 0-way and 2-way protocols, even in a very competitive network. The main reason for this is that no retransmission attempt is "wasted" when the receiver is not facing the transmitter, i.e, unless the transmitter has recently received a CTS packet from the intended receiver. However, this is not the case for 0-way and 2-way handshake protocols.

The cost of a lower discard probability is reflected in the achievable throughput, which is illustrated in Figs. 4a and 4c, from which we observe that the throughput achieved by 0-way or 2-way protocols is much lower than that of the proposed 1-way protocol. This mainly is because the two traditional protocols have extremely high packet discard probabilities and, thus, experience longer retransmission delays. In Fig. 4a, the comparatively larger throughput value bar of the proposed 1-way protocol also illustrates that, from another point of view, it wouldn't easily send out the DATA packets as the two traditional protocols do. The mechanism of waiting for the CTS packet guarantees a high successful transmission probability, but, on the other hand, extends the delay duration of some unfortunate transmissions that transmitters have to wait several sector times or even one round duration to meet the receiver.

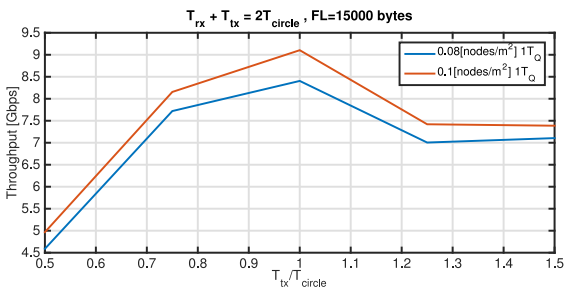

Fig. 5. Ad-hoc network architecture: Throughput as a function of time allocation.

6.1.2 Ad-hoc Network Architecture

As shown in Fig. 5, the *ns*-3 simulation results suggest that the maximum throughput is achieved when equally allocating *RM* duration and *TM* duration, which verifies our numerical analysis. In order to achieve the maximum throughput, we always equally allocate *TM* time and *RM* time resources for the following tests.

In Figs. 6b and 6d, we observe that with the proposed 1-way handshake protocol, the probability of discarding a packet is virtually zero and significantly much lower than 0-way and 2-way protocols. Mainly because the 1-way protocol can prevent "wasted" retransmission attempts as illustrated before. Meanwhile, more potential receivers occurring in the ad-hoc network architecture share the burden of channel contention and, thus, further reduce the packet collision probability.

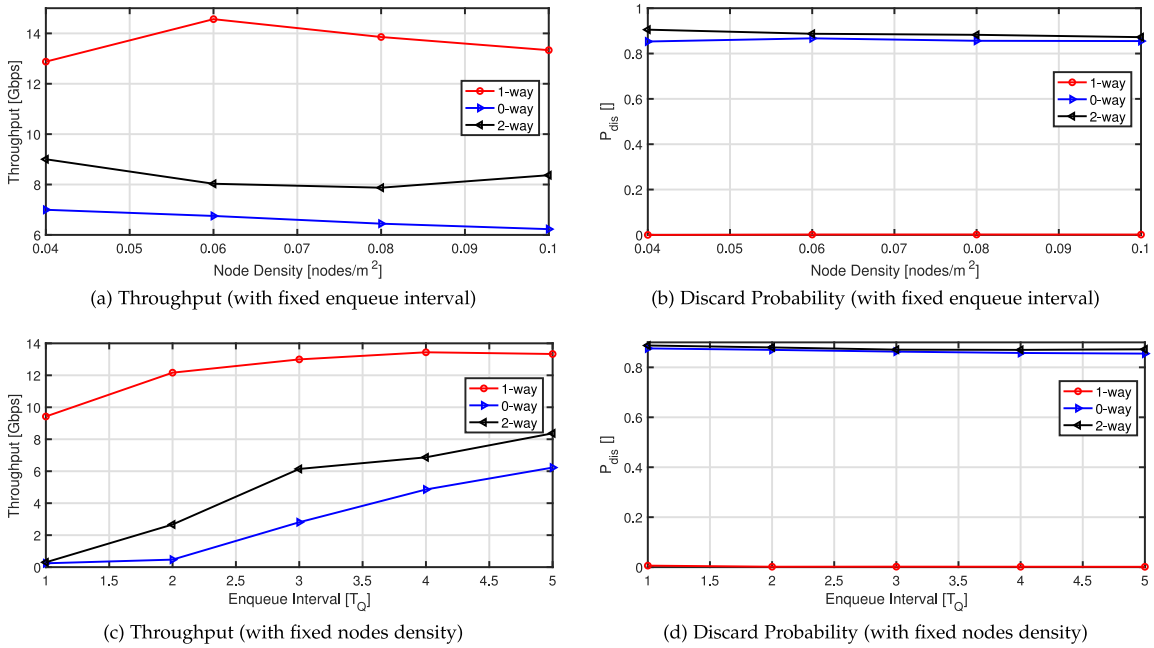

(a) Throughput (with fixed enqueue interval)
(b) Discard Probability (with fixed enqueue interval)
(c) Throughput (with fixed nodes density)
(d) Discard Probability (with fixed nodes density)

Fig. 6. Ad-hoc network architecture: Throughput and discard probability.

As shown in Fig. 6a, the throughput of the 1-way protocol is a function of node density. With a sustainable enqueue rate, the throughput of our proposed 1-way protocol shows a steady performance with increase of node density. In Fig. 6c, the throughput is a function of the DATA packet enqueue interval. The faster the packets are enqueued, the easier they are accumulated in the buffer and, thus, experience longer queuing delay. From both figures, we observe that the throughput achieved by 0-way or 2-way protocols are much lower than the throughput achieved by the proposed 1-way protocol.

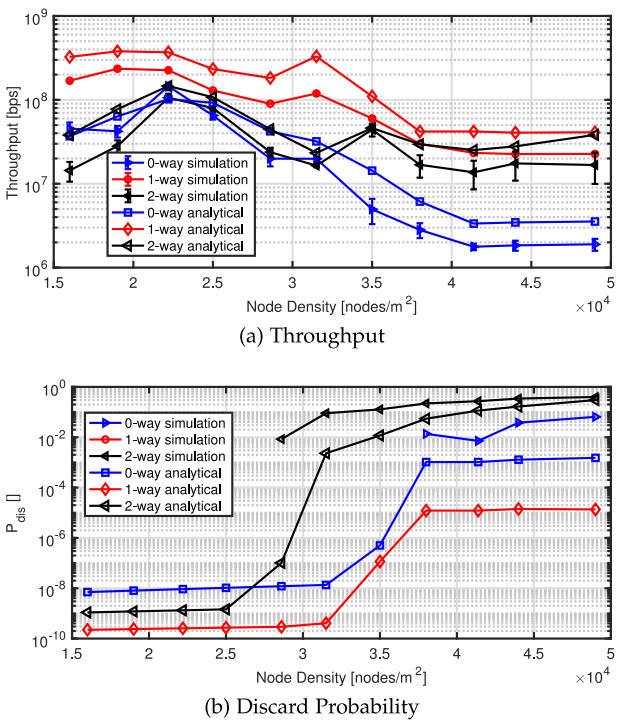

(a) Throughput
(b) Discard Probability

Fig. 7. Centralized network architecture: Throughput and discard probability as a function of the nodes density.

6.2 Nanoscale Scenario

In this case, we utilize the following parameter values. A circular area with radius $l = 0.01$ m with varying nano-device densities is considered. Nano-devices communicate by utilizing TS-OOK with pulse energy E^{tx}_{pulse}=1 attoJoule (aJ), pulse length T_p=100 fs, and spreading factor $T_s/T_p = 100$. Nodes utilize omnidirectional antennas with no directivity gain. For the energy model, we define an energy packet to be the amount of energy required to receive a control packet of length 17 bytes and energy harvesting interval $1/\lambda_{harv} = 8$ μs per energy packet. The capacity of the battery is ϵ_{max} = 1000 energy packets. We also consider that nano-devices generate packets of length 128 bytes and apply a coding weight $W = 0.5$.

6.2.1 *Centralized Network Architecture*

In the centralized network architecture, we consider that nano-controller harvest energy at a faster rate (3 μs per energy packet) to realize the fact that they have usually more resources than the sender nodes. As shown in Fig. 7b, the DATA packet discard probability for centralized network architecture is a function of the node density. Similarly as for the macroscale scenario, the number of dropped packets is significantly lower than that in the other protocols. Initially the discard probability is very low for all three protocols due to nano-controller serving fewer nodes. However, it increases sharply for the 2-way and 0-way protocols as the node density increases. It is relevant to note that in this case, the 0-way handshake protocol has a lower discard probability than the 2-way case. The reason for this is that the 2-way protocol counts the RTS failure towards the maximum number of retransmissions before dropping a packet. For the 0-way protocol, the retransmission happens due only to

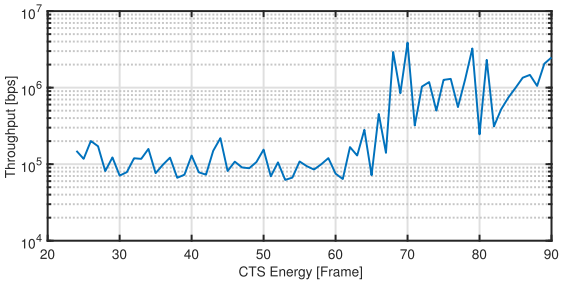

Fig. 8. Throughput as a function of the number of energy packets harvested before sending a CTS.

failed data packet transmission. As a result for every transmission wasted, the time duration before the next retransmission is very long for 0-way compared to that of the 2-way protocol. This can be seen in Fig. 7a, where the throughput is shown as a function of the node density. The throughput in the nanoscale scenario is much lower than that of the macroscale scenario due to the extra delay caused by energy harvesting. Even though our protocol utilizes backoff time before transmission to avoid packet loss, the throughput for our proposed protocol is significantly higher than for the other two protocols (note the logarithmic scale). The reason is again related to the very long time needed for a node to have enough energy to transmit after a failed transmission. This emphasizes the need for transmitter-receiver synchronization, which is satisfied by the 1-way handshake.

6.2.2 Ad-hoc Network Architecture

For the ad-hoc network architecture, we first determine at what energy level the node should send a CTS to increase the throughput while waiting to harvest enough energy to transmit. Fig. 8 depicts throughput as a function of energy levels required to send a CTS packet.

As can be seen from the figure, the throughput increases if the node waits to harvest enough energy to transmit before sending a CTS. The reason for this behavior is that when the nodes in *RM* send CTS before harvesting enough energy to transmit, the nodes in *TM* may not have enough energy and, thus, the energy to send the CTS is wasted. This can introduce more delays for a packet and the throughput is decreased in turn.

In the ad-hoc network architecture, each node has the same capabilities and harvests energy at the same rate (8 μs per energy packet). Moreover, unlike the centralized case, every node needs to both transmit and receive packets simultaneously. As a result, the throughput for the ad-hoc case is lower than that of the centralized architecture as shown in Fig. 9a. However, the throughput for 1-way protocol is still higher than that of the 0-way and 2-way protocols for the reasons explained before. Unlike the centralized network architecture, the discard probability is high from the beginning, as there is an energy issue right from the beginning in the ad-hoc case. As can be seen in Fig. 9b, the 1-way protocol has a zero discard probability. The reason for this is that 1-way prevents transmissions when the receiver is not ready. The random backoff after receiving the CTS further ensures that nodes do not send more packets than the receiver can handle with its available energy. In addition, the discard probability

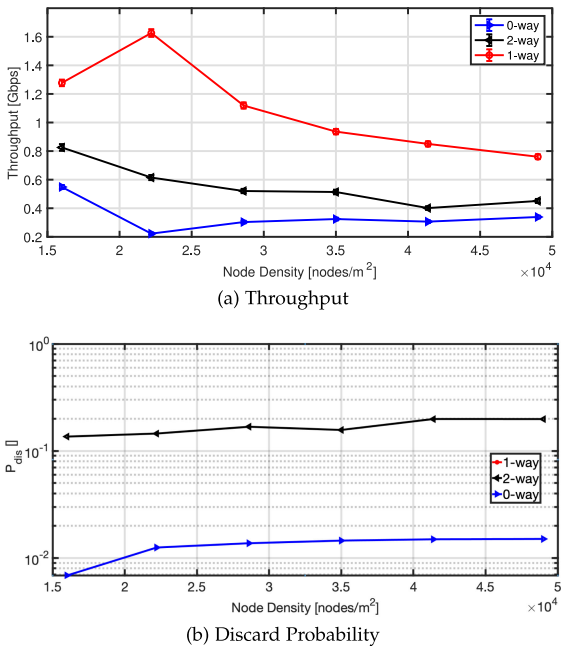

Fig. 9. Ad-hoc network architecture: Throughput and discard probability as functions of the nodes density.

for the 2-way protocol is again higher than that of 0-way case for the reasons mentioned earlier.

7 Conclusion

In this paper, we have presented a link-layer synchronization and MAC protocol for ultra-high-speed wireless communication networks in the THz band. The protocol relies on a receiver-initiated handshake as well as an aggregated packet or a sliding window flow control mechanism to guarantee synchronization between transmitter and receiver, maximizes the channel utilization and minimizes the packet discard probability. The performance of the proposed protocol is analytically investigated, compared to that of a modified CSMA/CA with and without RTS/CTS, and validated though extensive simulations with *ns*-3. The results show that the proposed protocol can maximize the successful packet delivery probability and enhance the achievable throughput in THz-band communication networks.

Acknowledgments

(a) The State University of New York at Buffalo acknowledges the U.S. Government's support in the publication of this paper. This material is based upon work funded by AFRL, under AFRL Grant No. FA8750-15-1-0050. (b) Any opinions, findings, and conclusions or recommendations expressed in this material are those of the author(s) and do not necessarily reflect the views of AFRL.

References

[1] "Cisco visual networking index: Global mobile data traffic forecast update," 2017–2022 white paper. [Online]. Available: https://www.cisco.com/c/en/us/solutions/collateral/service-provider/visual-networking-index-vni/white-paper-c11-738429.html

[2] J. Federici and L. Moeller, "Review of terahertz and subterahertz wireless communications," *J. Appl. Physics*, vol. 107, no. 11, 2010, Art. no. 111101.

[3] H. Song and T. Nagatsuma, "Present and future of terahertz communications," *IEEE Trans. Terahertz Sci. Technol.*, vol. 1, no. 1, pp. 256–263, Sep. 2011.
[4] I. F. Akyildiz, J. M. Jornet, and C. Han, "Terahertz band: Next frontier for wireless communications," *Phys. Commun. J.*, vol. 12, pp. 16–32, Sep. 2014.
[5] T. Kurner and S. Priebe, "Towards THz communications-status in research, standardization and regulation," *J. Infrared Millimeter. Terahertz Waves*, vol. 35, no. 1, pp. 53–62, 2014.
[6] K. Sengupta, T. Nagatsuma, and D. M. Mittleman, "Terahertz integrated electronic and hybrid electronic–photonic systems," *Nature Electronics*, vol. 1, no. 12, 2018, Art. no. 622.
[7] A. Nikpaik, A. H. M. Shirazi, A. Nabavi, S. Mirabbasi, and S. Shekhar, "A 219-to-231 GHz frequency-multiplier-based VCO with 3% peak DC-to-RF efficiency in 65-nm CMOS," *IEEE J. Solid-State Circuits*, vol. 53, no. 2, pp. 389–403, Feb. 2018.
[8] H. Aghasi, A. Cathelin, and E. Afshari, "A 0.92-THz sige power radiator based on a nonlinear theory for harmonic generation," *IEEE J. Solid-State Circuits*, vol. 52, no. 2, pp. 406–422, Feb. 2017.
[9] W. R. Deal, K. Leong, A. Zamora, B. Gorospe, K. Nguyen, and X. B. Mei, "A 660 GHz up-converter for THz communications," in *Proc. IEEE Compound Semicond. Integr. Circuit Symp.*, 2017, pp. 1–4.
[10] A. Leuther, A. Tessmann, P. Doria, M. Ohlrogge, M. Seelmann-Eggebert, H. Maßler, M. Schlechtweg, and O. Ambacher, "20 nm metamorphic HEMT technology for terahertz monolithic integrated circuits," in *Proc. 9th IEEE Eur. Microw. Integr. Circuit Conf.*, 2014, pp. 84–87.
[11] M. Urteaga, Z. Griffith, M. Seo, J. Hacker, and M. J. Rodwell, "InP HBT technologies for THz integrated circuits," *Proc. IEEE*, vol. 105, no. 6, pp. 1051–1067, Jun. 2017.
[12] I. Mehdi, J. V. Siles, C. Lee, and E. Schlecht, "THz diode technology: Status, prospects, and applications," *Proc. IEEE*, vol. 105, no. 6, pp. 990–1007, Jun. 2017.
[13] H.-J. Song, K. Ajito, Y. Muramoto, A. Wakatsuki, T. Nagatsuma, and N. Kukutsu, "Uni-travelling-carrier photodiode module generating 300 GHz power greater than 1 mW," *IEEE Microw. Wireless Compon. Lett.*, vol. 22, no. 7, pp. 363–365, Jul. 2012.
[14] S.-W. Huang, J. Yang, S.-H. Yang, M. Yu, D.-L. Kwong, T. Zelevinsky, M. Jarrahi, and C. W. Wong, "Globally stable microresonator turing pattern formation for coherent high-power THz radiation on-chip," *Phys. Rev. X*, vol. 7, no. 4, 2017, Art. no. 041002.
[15] T. Nagatsuma, G. Ducournau, and C. C. Renaud, "Advances in terahertz communications accelerated by photonics," *Nature Photon.*, vol. 10, no. 6, 2016, Art. no. 371.
[16] Q. Lu, D. Wu, S. Sengupta, S. Slivken, and M. Razeghi, "Room temperature continuous wave, monolithic tunable THz sources based on highly efficient mid-infrared quantum cascade lasers," *Sci. Reports*, vol. 6, 2016, Art. no. 23595.
[17] K. S. Novoselov, V. Fal, L. Colombo, P. Gellert, M. Schwab, K. Kim, et al., "A roadmap for graphene," *Nature*, vol. 490, no. 7419, pp. 192–200, 2012.
[18] A. C. Ferrari, F. Bonaccorso, V. Fal'Ko, K. S. Novoselov, S. Roche, P. Bøggild, S. Borini, F. H. Koppens, V. Palermo, N. Pugno, et al., "Science and technology roadmap for graphene, related two-dimensional crystals, and hybrid systems," *Nanoscale*, vol. 7, no. 11, pp. 4598–4810, 2015.
[19] J. M. Jornet and I. F. Akyildiz, "Channel modeling and capacity analysis of electromagnetic wireless nanonetworks in the terahertz band," *IEEE Trans. Wireless Commun.*, vol. 10, no. 10, pp. 3211–3221, Oct. 2011.
[20] S. Priebe and T. Kurner, "Stochastic modeling of THz indoor radio channels," *IEEE Trans. Wireless Commun.*, vol. 12, no. 9, pp. 4445–4455, Sep. 2013.
[21] S. Koenig, D. Lopez-Diaz, J. Antes, F. Boes, R. Henneberger, A. Leuther, A. Tessmann, R. Schmogrow, D. Hillerkuss, R. Palmer, et al., "Wireless sub-THz communication system with high data rate," *Nature Photonics*, vol. 7, no. 12, pp. 977–981, 2013.
[22] E. Khorov, A. Kiryanov, A. Lyakhov, and G. Bianchi, "A tutorial on ieee 802.11ax high efficiency WLANs," *IEEE Commun. Surveys Tutorials*, vol. 21, no. 1, pp. 197–216, Jan.-Mar. 2019.
[23] Y. Ghasempour, C. R. C. M. da Silva, C. Cordeiro, and E. W. Knightly, "IEEE 802.11ay: Next-generation 60 GHz communication for 100 Gb/s Wi-Fi," *IEEE Commun. Mag.*, vol. 55, no. 12, pp. 186–192, Dec. 2017.
[24] "IEEE Standard for High Data Rate Wireless Multi-Media Networks–Amendment 2: 100 Gb/s Wireless Switched Point-to-Point Physical Layer", in *IEEE Std 802.15.3d-2017 (Amendment to IEEE Std 802.15.3-2016 as amended by IEEE Std 802.15.3e-2017)*, pp. 1–55, Oct. 18, 2017. doi: 10.1109/IEEESTD.2017.8066476.
[25] V. Radisic, K. Leong, D. Scott, C. Monier, X. Mei, W. Deal, and A. Gutierrez-Aitken, "Sub-millimeter wave InP technologies and integration techniques," in *Proc. IEEE MTT-S Int. Microw. Symp.*, May 2015, pp. 1–4.
[26] S. Slivken and M. Razeghi, "High power, electrically tunable quantum cascade lasers," in *SPIE OPTO*. Bellingham, WA, USA: International Society for Optics and Photonics, 2016, vol. 9755, pp. 97 550C–97 550C. doi: 10.1117/12.2216304.
[27] S. Singh, R. Mudumbai, and U. Madhow, "Interference analysis for highly directional 60-GHz mesh networks: The case for rethinking medium access control," *IEEE/ACM Trans. Netw.*, vol. 19, no. 5, pp. 1513–1527, Oct. 2011.
[28] M. X. Gong, R. Stacey, D. Akhmetov, and S. Mao, "A directional CSMA/CA protocol for mmWave wireless PANs," in *Proc. IEEE Wireless Commun. Netw. Conf.*, Apr. 2010, pp. 1–6.
[29] M. Takata, M. Bandai, and T. Watanabe, "A receiver-initiated directional MAC protocol for handling deafness in Ad Hoc networks," in *Proc. IEEE Int. Conf. Commun.*, 2006, vol. 9, pp. 4089–4095.
[30] P. Bai, G. Zhu, Y. Liu, J. Chen, Q. Jing, W. Yang, J. Ma, G. Zhang, and Z. L. Wang, "Cylindrical rotating triboelectric nanogenerator," *ACS Nano*, vol. 7, no. 7, pp. 6361–6366, 2013.
[31] A. Gupta, M. Medley, and J. M. Jornet, "Joint synchronization and symbol detection design for pulse-based communications in the THz band," in *Proc. IEEE Global Commun. Conf.*, Dec. 2015, pp. 1–7.
[32] Z. Hossain, Q. Xia, and J. M. Jornet, "TeraSim: An ns-3 extension to simulate terahertz-band communication networks," *Nano Commun. Netw.*, vol. 17, pp. 36–44, 2018.
[33] A. Akhtar and S. C. Ergen, "Directional MAC protocol for IEEE 802.11ad based wireless local area networks," *Ad Hoc Netw.*, vol. 69, pp. 49–64, 2018.
[34] Q. Chen, J. Tang, D. T. C. Wong, X. Peng, and Y. Zhang, "Directional cooperative MAC protocol design and performance analysis for IEEE 802.11ad WLANs," *IEEE Trans. Veh. Technol.*, vol. 62, no. 6, pp. 2667–2677, Jul. 2013.
[35] R. R. Choudhury, X. Yang, R. Ramanathan, and N. H. Vaidya, "On designing MAC protocols for wireless networks using directional antennas," *IEEE Trans. Mobile Comput.*, vol. 5, no. 5, pp. 477–491, May 2006.
[36] E. Shihab, L. Cai, and J. Pan, "A distributed asynchronous directional-to-directional MAC protocol for wireless Ad Hoc networks," *IEEE Trans. Veh. Technol.*, vol. 58, no. 9, pp. 5124–5134, Nov 2009.
[37] L. X. Cai, L. Cai, X. Shen, and J. W. Mark, "Rex: A randomized EXclusive region based scheduling scheme for mmWave WPANs with directional antenna," *IEEE Trans. Wireless Commun.*, vol. 9, no. 1, pp. 113–121, Jan. 2010.
[38] C. S. Sum and H. Harada, "Scalable heuristic STDMA scheduling scheme for practical multi-gbps millimeter-wave WPAN and WLAN systems," *IEEE Trans. Wireless Commun.*, vol. 11, no. 7, pp. 2658–2669, Jul. 2012.
[39] I. K. Son, S. Mao, M. X. Gong, and Y. Li, "On frame-based scheduling for directional mmwave WPANs," in *Proc. IEEE INFOCOM*, Mar. 2012, pp. 2149–2157.
[40] P. Bjorklund, P. Varbrand, and D. Yuan, "Resource optimization of spatial TDMA in Ad Hoc radio networks: A column generation approach," in *Proc. 22nd Annu. Joint Conf. IEEE Comput. Commun. Societies*, Mar. 2003, pp. 818–824.
[41] Y. Niu, L. Su, C. Gao, Y. Li, D. Jin, and Z. Han, "Exploiting device-to-device communications to enhance spatial reuse for popular content downloading in directional mmwave small cells," *IEEE Trans. Veh. Technol.*, vol. 65, no. 7, pp. 5538–5550, Jul. 2016.
[42] "IEEE standard for information technology–Local and metropolitan area networks–Specific requirements–Part 15.3: Amendment 2: Millimeter-wave-based alternative physical layer extension," in *IEEE Std 802.15.3c-2009 (Amendment to IEEE Std 802.15.3-2003)*, pp. 1–200, Oct. 12, 2009. doi: 10.1109/IEEESTD.2009.5284444.
[43] S. Jin, M. Choi, K. Kim, and S. Choi, "Opportunistic spatial reuse in IEEE 802.15.3c wireless personal area networks," *IEEE Trans. Veh. Technol.*, vol. 62, no. 2, pp. 824–834, Feb. 2013.

[44] T. Baykas, C. S. Sum, Z. Lan, J. Wang, M. A. Rahman, H. Harada, and S. Kato, "IEEE 802.15.3c: The first IEEE wireless standard for data rates over 1 Gb/s," *IEEE Commun. Mag.*, vol. 49, no. 7, pp. 114–121, Jul. 2011.
[45] X. An and R. Hekmat, "Directional MAC protocol for millimeter wave based wireless personal area networks," in *Proc. IEEE Veh. Technol. Conf.*, May 2008, pp. 1636–1640.
[46] "IEEE standard for information technology–Telecommunications and information exchange between systems–Local and metropolitan area networks–Specific requirements-Part 11: Wireless LAN Medium Access Control (MAC) and Physical Layer (PHY) specifications amendment 3: Enhancements for very high throughput in the 60 GHz band," in *IEEE Std 802.11ad-2012 (Amendment to IEEE Std 802.11-2012, as amended by IEEE Std 802.11ae-2012 and IEEE Std 802.11aa-2012)*, pp. 1–628, Dec. 28, 2012. doi: 10.1109/IEEESTD.2012.6392842.
[47] T. Nitsche, C. Cordeiro, A. B. Flores, E. W. Knightly, E. Perahia, and J. C. Widmer, "IEEE 802.11ad: Directional 60 GHz communication for multi-gigabit-per-second Wi-Fi [invited paper]," *IEEE Commun. Mag.*, vol. 52, no. 12, pp. 132–141, Dec. 2014.
[48] Y. Ghasempour, C. R. C. M. da Silva, C. Cordeiro, and E. W. Knightly, "IEEE 802.11ay: Next-generation 60 GHz communication for 100 Gb/s Wi-Fi," *IEEE Commun. Mag.*, vol. 55, no. 12, pp. 186–192, Dec. 2017.
[49] P. Zhou, K. Cheng, X. Han, X. Fang, Y. Fang, R. He, Y. Long, and Y. Liu, "IEEE 802.11ay based mmwave WLANs: Design challenges and solutions," *IEEE Commun. Surveys Tutorials*, vol. 20, no. 3, pp. 1654–1681, Jul.-Aug. 2018.
[50] X.-W. Yao and J. M. Jornet, "TAB-MAC: Assisted beamforming MAC protocol for terahertz communication networks," *Nano Commun. Netw.*, vol. 9, pp. 36–42, 2016.
[51] J. M. Jornet, J. C. Pujol, and J. S. Pareta, "PHLAME: A physical layer aware MAC protocol for electromagnetic nanonetworks in the terahertz band," *Nano Commun. Netw. J.*, vol. 3, no. 1, pp. 74–81, 2012.
[52] P. Wang, J. M. Jornet, M. Abbas Malik, N. Akkari, and I. F. Akyildiz, "Energy and spectrum-aware MAC protocol for perpetual wireless nanosensor networks in the terahertz band," *Ad Hoc Netw. J.*, vol. 11, no. 8, pp. 2541–2555, 2013.
[53] S. Mohrehkesh and M. C. Weigle, "RIH-MAC: Receiver-initiated harvesting-aware MAC for nanonetworks," in *Proc. ACM 1st Annu. Int. Conf. Nanoscale Comput. Commun.*, 2014, pp. 1–9.
[54] J. M. Jornet and I. F. Akyildiz, "Femtosecond-long pulse-based modulation for terahertz band communication in nanonetworks," *IEEE Trans. Commun.*, vol. 62, no. 5, pp. 1742–1754, May 2014.
[55] Q. Xia, Z. Hossain, M. Medley, and J. M. Jornet, "A link-layer synchronization and medium access control protocol for terahertz-band communication networks," in *Proc. IEEE Global Commun. Conf.*, Dec. 2015, pp. 1–7.
[56] J. M. Jornet, "Low-weight error-prevention codes for electromagnetic nanonetworks in the terahertz band," *Nano Commun. Netw. J.*, vol. 5, no. 1–2, pp. 35–44, Mar.-Jun. 2014.
[57] C. A. Balanis, *Antenna Theory: Analysis and Design*. Hoboken, NJ, USA: Wiley, 2005.
[58] K. Sengupta and A. Hajimiri, "A 0.28 THz power-generation and beam-steering array in CMOS based on distributed active radiators," *IEEE J. Solid-State Circuits*, vol. 47, no. 12, pp. 3013–3031, Dec. 2012.
[59] I. F. Akyildiz and J. M. Jornet, "Realizing ultra-massive MIMO (1024× 1024) communication in the (0.06–10) terahertz band," *Nano Commun. Netw.*, vol. 8, pp. 46–54, 2016.
[60] K. Sengupta and A. Hajimiri, "Sub-THz beam-forming using near-field coupling of distributed active radiator arrays," in *Proc. IEEE Radio Frequency Integr. Circuits Symp.*, 2011, pp. 1–4.
[61] N. Thawdar, M. Andrello, III, and J. M. Jornet, "Modeling and performance analysis of a reconfigurable plasmonic nano-antenna array architecture for terahertz communications," in *Proc. 5th ACM Int. Conf. Nanoscale Comput. Commun.*, 2018, pp. 20:1–20:6.
[62] A. Akatay and H. Urey, "Design and optimization of microlens array based high resolution beam steering system," *Optics Exp.*, vol. 15, no. 8, pp. 4523–4529, 2007.
[63] M. Alonso-delPino, C. Jung-Kubiak, T. Reck, N. Llombart, and G. Chattopadhyay, "Beam scanning of silicon lens antennas using integrated piezomotors at submillimeter wavelengths," *IEEE Trans. Terahertz Sci. Technol.*, vol. 9, no. 1, pp. 47–54, Jan. 2019.
[64] J. M. Jornet and I. F. Akyildiz, "Joint energy harvesting and communication analysis for perpetual wireless nanosensor networks in the terahertz band," *IEEE Trans. Nanotechnol.*, vol. 11, no. 3, pp. 570–580, May 2012.
[65] S. Marinkovic and E. Popovici, "Nano-power wake-up radio circuit for wireless body area networks," in *Proc. IEEE Radio Wireless Symp.*, 2011, pp. 398–401.
[66] R. R. Choudhury, X. Yang, R. Ramanathan, and N. Vaidya, "On designing MAC protocols for wireless networks using directional antennas," *IEEE Trans. Mobile Comput.*, vol. 5, no. 5, pp. 477–491, May 2006.
[67] A. Patra, L. Simic, and M. Petrova, "Experimental evaluation of a novel fast beamsteering algorithm for link re-establishment in mm-wave indoor wlans," in *Proc. IEEE 27th Annu. Int. Symp. Pers. Indoor Mobile Radio Commun.*, Sep. 2016, pp. 1–7.
[68] G. M. Olcer, Z. Genc, and E. Onur, "Sector scanning attempts for non-isolation in directional 60 GHz networks," *IEEE Commun. Lett.*, vol. 14, no. 9, pp. 845–847, Sep. 2010.
[69] Q. Xia and J. M. Jornet, "Expedited neighbor discovery in directional terahertz communication networks enhanced by antenna side-lobe information," *IEEE Trans. Veh. Technol.*, vol. 68, no. 8, pp. 7804–7814, Aug. 2019.
[70] P.-Y. Chen and A. Alù, "THz beamforming using graphene-based devices," in *Proc. IEEE 13th Top. Meet. Silicon Monolithic Integr. Circuits RF Syst.*, 2013, pp. 36–38.
[71] R. Bonjour, M. Burla, F. C. Abrecht, S. Welschen, C. Hoessbacher, W. Heni, S. A. Gebrewold, B. Baeuerle, A. Josten, Y. Salamin, C. Haffner, P. V. Johnston, D. L. Elder, P. Leuchtmann, D. Hillerkuss, Y. Fedoryshyn, L. R. Dalton, C. Hafner, and J. Leuthold, "Plasmonic phased array feeder enabling ultra-fast beam steering at millimeter waves," *Opt. Exp.*, vol. 24, no. 22, pp. 25 608–25 618, Oct. 2016.
[72] Z. Hossain, Q. Xia, and J. M. Jornet, "Terasim: An ns-3 extension to simulate terahertz-band communication networks," *Nano Commun. Netw.*, vol. 17, pp. 36–44, 2018.

Qing Xia received the BS degree in electrical engineering from the Hebei University of Technology, Tianjin, China, in 2010, the MS degree in electrical engineering from the University of Denver, CO, in 2012, and the PhD degree in electrical engineering from the University at Buffalo, the State University of New York (UB), in 2019. She was an intern at Intel Lab, OR, in 2016. Currently, she is working as senior wireless research engineer at the Sony Corporation of America. This work was completed at the University at Buffalo, as part of her PhD work under the supervision of Prof. Josep M. Jornet. Her current research interests include protocol design, network simulator development and performance analysis, Terahertz-band communication networks, millimeter wave communication networks, and IoT. She is a student member of the IEEE.

Zahed Hossain received the BS degree in electronic and telecommunication engineering from North South University, Bangladesh, in 2010, and the MS and PhD degrees in electrical engineering from the University at Buffalo, The State University of New York, UB, in 2014 and 2018, respectively. From January 2010 to August 2012, he worked as a lab instructor at the same university. He has worked as a lecturer in the same department and taught signals and systems in the Summer of 2014-2017. He was the recipient of the Best Paper Award for ACM NanoCom in 2017. Currently, he is working as a wireless standards systems engineer at the Intel Corporation. This work was completed at the University at Buffalo, as part of his PhD work under the supervision of Prof. Josep M. Jornet. His current research interests include modulation, channel modeling, multi-user interference modeling, protocol design, performance analysis and network simulation for Terahertz-band communication networks, with applications in terabit wireless personal and local area networks, next generation small cells, wireless nanosensor networks, and the internet of nano-things. He is a student member of the IEEE

Michael J. Medley (M'91-SM'02) received the BS, MS, and PhD degrees in electrical engineering from the Rensselaer Polytechnic Institute, Troy, NY, in 1990, 1991, and 1995, respectively. Since 1991, he has been a research engineer for the United States Air Force at the Air Force Research Laboratory, Rome, NY, where he has been involved in communications and signal processing research related to adaptive interference suppression, spread spectrum waveform design, spectrum management, covert messaging, and airborne networking and communications links. In 2002, he joined the State University of New York Polytechnic Institute in Utica, NY, where he currently serves as an associate professor in the Electrical and Computer Engineering Department. He is a senior member of the IEEE.

Josep M. Jornet received the BS degree in telecommunication engineering and the MSc degree in information and communication technologies from the Universitat Politecnica de Catalunya, Barcelona, Spain, in 2008, and the PhD degree in electrical and computer engineering from the Georgia Institute of Technology (Georgia Tech), Atlanta, GA, in 2013. From September 2007 to December 2008, he was a visiting researcher at the Massachusetts Institute of Technology (MIT), Cambridge, under the MIT Sea Grant program. Between August 2013 and August 2019, he was a faculty with the Department of Electrical Engineering, University at Buffalo, The State University of New York. Since August 2019, he has been an associate professor with the Department of Electrical and Computer Engineering, Northeastern University, in Boston, MA. His current research interests are in terahertz-band communication networks, wireless nano-bio-communication networks, and the internet of nano-things. In these areas, he has co-authored more than 120 peer-reviewed scientific publications, one book, and has also been granted three US patents. Since July 2016, he has been the editor-in-chief of the *Nano Communication Networks* (Elsevier) *Journal*. He is serving as the lead PI on multiple grants from U.S. federal agencies including the National Science Foundation, the Air Force Office of Scientific Research, and the the Air Force Research Laboratory. He is a recipient of the National Science Foundation CAREER award and of several other awards from the IEEE, ACM, and UB. He is a member of the IEEE.